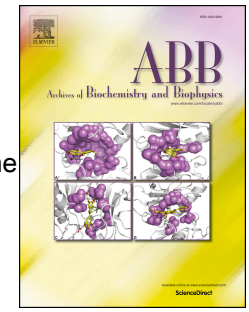

Electron transfer and conformational transitions of cytochrome *c* are modulated by the same dynamical features

Santiago Oviedo-Rouco, Juan Manuel Perez-Bertoldi, Celicia Spedalieri, María A. Castro, Florencia Tomasina, Verónica Tortora, Rafael Radi, Daniel H. Murgida

PII: S0003-9861(19)31061-6

DOI: https://doi.org/10.1016/j.abb.2019.108243

Reference: YABBI 108243

To appear in: *Archives of Biochemistry and Biophysics*

Received Date: 16 November 2019

Revised Date: 11 December 2019

Accepted Date: 29 December 2019

Please cite this article as: S. Oviedo-Rouco, J.M. Perez-Bertoldi, C. Spedalieri, Marí.A. Castro, F. Tomasina, Veró. Tortora, R. Radi, D.H. Murgida, Electron transfer and conformational transitions of cytochrome *c* are modulated by the same dynamical features, *Archives of Biochemistry and Biophysics* (2020), doi: https://doi.org/10.1016/j.abb.2019.108243.

S. Oviedo-Rouco: conceptualization, methodology, investigation, writing

J.M. Perez-Bertoldi: investigation

C. Spedalieri: investigation

M.A. Castro: investigation, writing

F. Tomasina: investigation

V. Tórtora: investigation

R. Radi: supervision, writing

D.H. Murgida: conceptualization, supervision, writing

Electron transfer and conformational transitions of cytochrome *c* are modulated by the same dynamical features

Santiago Oviedo-Rouco,[†] *Juan Manuel Perez-Bertoldi,*[†] *Celicia Spedalieri,* [†] *María A. Castro,*[†] *Florencia Tomasina,*[‡] *Verónica Tortora,*[‡] *Rafael Radi,*[‡] *and Daniel H. Murgida*[†]*

[†]Departamento de Química Inorgánica, Analítica y Química Física and INQUIMAE (CONICET-UBA), Facultad de Ciencias Exactas y Naturales, Universidad de Buenos Aires, Ciudad Universitaria, Pab. 2, piso 1, Buenos Aires C1428EHA, Argentina

[‡]Departamento de Bioquímica and Centro de Investigaciones Biomédicas (CEINBIO), Facultad de Medicina, Universidad de la Republica, Av. Gral. Flores 2125, Montevideo 11800, Uruguay

*Corresponding Author: E-mail: dhmurgida@qi.fcen.uba.ar Phone.: +54-11-5285-8208

ORCID Daniel H. Murgida: 0000-0001-5173-0183

Keywords: cytochrome *c*, alkaline transition, time-resolved SERR, protein nitration, protein dynamics, protein electron transfer

ABSTRACT

Cytochrome *c* is a prototypical multifunctional protein that is implicated in a variety of processes that are essential both for sustaining and for terminating cellular life. Typically, alternative functions other than canonical electron transport in the respiratory chain are associated to alternative conformations. In this work we apply a combined experimental and computational study of Cyt c variants to assess whether the parameters that regulate the canonical electron transport function of Cyt c are correlated with those that determine the transition to alternative conformations, using the alkaline transition as a model conformational change. The results show that pK_a values of the alkaline transition correlate with the activation energies of the frictionally-controlled electron transfer reaction, and that both parameters are mainly modulated by the flexibility of the Ω-loop 70-85. Reduction potentials and non-adiabatic ET reorganization energies, on the other hand, are both modulated by the flexibilities of the Ω-loops 40-57 and 70-85. Finally, all the measured thermodynamic and kinetic parameters that characterize both types of processes exhibit systematic variations with the dynamics of the hydrogen bond between the axial ligand Met80 and the second sphere ligand Tyr67, thus highlighting the critical role of Tyr67 in controlling canonical and alternative functions of Cyt c.

1. INTRODUCTION

Cytochrome *c* (Cyt c) is a small, cationic and soluble monohemic protein, whose canonical function is shuttling electrons in mitochondrial respiratory chains.[1] This function is exerted by the so-called native protein conformation that at neutral pH has a characteristic Met80/His18 axial coordination pattern of the heme iron.[2,3] In addition to electron transfer (ET), a variety of alternative functions of Cyt c have been recently documented,[4] including cardiolipin peroxidation,[5] apoptosome assembly[6] and histone chaperone inhibition,[7] thus pointing out

Cyt c as a prototypical moonlighting protein.[8] Conformational changes that lead to the gain of alternative peroxidase function have been found to be triggered by a variety of stimuli such as post-translational modifications,[9–21] interactions with cardiolipin,[22,23] naturally or artificially occurring mutations,[16,21,24,25] pH changes[26,27] and local electric fields.[28] A feature common to most of these transitions is the disruption of the Fe-Met80 bond, which may lead to different axial coordination patterns depending on the specific conditions. For example, the so-called alkaline transition leads to the pH-induced replacement of Met80 by either Lys73 or Lys79.[29] This transition takes place with pK_a 9.4 for WT Cyt c in solution, but it shifts towards physiological pH for point mutants found in human patients and others,[16,21,24,25,30,31] as well as upon several post-translational modifications,[10,13–21] including nitration of Tyr74 under oxidative stress (NO_2-Cyt c hereafter),[11,12,32] thus suggesting potential physiological relevance for the Met/Lys conformer. Moreover, the alkaline transition constitutes an excellent model for studying the structural and dynamic basis of Cyt c multifunctionality in general. The thermodynamic and kinetic redox properties of Cyt c[1,33–35] as well as structural and dynamical aspects of the native and alternative conformations[4,29,36–38] have been studied at length. Based on the available information one can reason out that the basis for Cyt c multifunctionality is its high flexibility, which enables exploration of a broad conformational space. This leads us to the still unverified working hypothesis that redox and conformational parameters should be somehow cross-correlated. Here we address this issue by a combination of experimental and computational methods that unveil the intertwining between thermodynamic and kinetic ET parameters and the pK_a´s of alkaline transitions. The different magnitudes were found to be modulated by flexibility of distinct structural elements, with a differential response depending on the ET regime, ie. nonadiabatic vs friction control.

2. MATERIALS AND METHODS

2.1. Chemicals. Horse heart cytochrome *c* BioUltra ≥99% (Cyt c), buffer CHES, 16-mercapto-1-hexadecanoic acid, 11-mercapto-1-undecanol, 11-mercapto-1-undecanoic, 8-hydroxy-1-octanethiol, 8-mercapto-1-octanoic acid, 6-mercaptohexan-1-ol, 6-mercapto-1-hexanoic acid, 4-mercapto-1-butanol, 4-mercaptobutiryc acid, polyethylene glycol average weight 4000 (PEG-4000), sucrose, N-cyclohexyl-N'-(2-morpholinoethyl) carbodiimide methyl-p-toluenesulfonate (CMC), N-hydroxysuccinimide (NHS), K_2HPO_4 and K_2SO_4 were purchased from Merck. 16-mercapto-1-hexadecanol was purchased from Frontier Scientific, Inc. All experiments were conducted with type II water (R > 18 MΩ).

2.2. Protein production. The mutants Y67F and E66Q, as well as the variants WT Cyt c and Y67F nitrated at Tyr74 (NO_2-Cyt c and NO_2-Y67F, respectively) were produced and purified following published procedures.[11,39]

2.3. UV-vis titrations. Absorption spectra were acquired with a Thermo Scientific Evolution Array spectrophotometer using 1 cm quartz cuvettes. Alkaline transitions were monitored following the disappearance of the band at 695 nm, ε_{695}= 865 $M^{-1}cm^{-1}$.

2.4. Molecular dynamics simulations. The initial Cyt c structure corresponds to ferric horse heart Cyt c, PDB 1HRC.[40] The Y67F, E66Q and NO_2-Cyt c variants were created *in silico* from WT Cyt c, and relaxed using standard procedures.[35]

All structures were optimized in a TIP3P water box and then heated and equilibrated at 300K, followed by a production run of 50 ns. Temperature and pressure were kept constant using the Berendsen thermostat and barostat.[41] For PBC simulations, Ewald summations were used to

compute the electrostatic energy terms using the default parameters in the PMEMD module of the AMBER16 package[42] with the ffSB14 force field implementation.[43]

Canonical H-bonds were evaluated using default values of the CPPTRAJ module of the AMBER16 package. For the atypical H-bond Y67-M80 we computed a score function based on the criteria defined by Zhou *et al*.[44] For each frame we evaluated five parameters that define the H-bond and assigned a value of one to each parameter that is within optimal range, thus yielding a final score between 0 (no H-bond) and 5 (optimal H-bond). For translating the scores into percentage of frames were the H-bond is present we adopted a cut-off score of 4.

2.4. Cyclic voltammetry. Electrochemical experiments were performed with a Gamry REF600 electrochemical workstation using a non-isothermal cell equipped with a polycrystalline gold bead working electrode, a Pt wire as counter electrode and Ag/AgCl (3.5 M KCl) reference electrode. Au electrodes were treated as described before[45] and coated with self-assembled monolayers (SAMs) by overnight incubation into 2 mM:2 mM ethanol solutions of HS-$(CH_2)_n$-CH_2OH : HS-$(CH_2)_n$-COOH mixtures (n= 4, 6, 8, 11 and 16). The SAM-coated electrodes were then incubated for 1 h into 400 μM protein solutions, then rinsed and inserted into the cell. Unless stated otherwise, determinations were performed in 12.5 mM phosphate buffer, pH=7.0, containing 12.5 mM K_2SO_4. Viscosities were adjusted with either sucrose or PEG-4000.

2.5. Raman spectroscopy and spectroelectrochemistry. Resonance Raman (RR) spectra were recorded in a Raman microscope (Dilor XY; f = 800 mm) equipped with CCD detection and 1800 l / mm grating. Increments per data point were typically 0.4 cm^{-1} and accumulation times were ca. 10-30 s. Spectra were acquired using either Soret band excitation (406 nm; TopMode-HP-406 diode laser; 3.5 mW at sample) or Q-band excitation (514 nm; Coherent

Innova 70c Ar laser; 13 mW at sample). Spectral calibration was done using either Hg and Na lamps or chemical standards (silicon and 4-acetamidophenol).

For measurements in solution samples were placed either in a cylindrical cuvette rotated at 10 Hz or in a standard spectrophotometric cuvette equipped with magnetic stirring. The set-up for stationary and time-resolved surface-enhanced resonance Raman (SERR) experiments was as described before.[27] Ag ring working electrodes were polished and subjected to oxidation-reduction cycles in 0.1 M KCl and incubated in 2 mM ethanolic solutions of the alkanethiols (1:1 mixtures of HS-$(CH_2)_n$-CH_2OH and HS-$(CH_2)_n$-COOH with n= 4, 6, 8, 11 and 16) for ca. 24 hs. SAM-coated electrodes were mounted on a shaft that was rotated at about 5 Hz to avoid laser-induced degradation. After background subtraction, RR and SERR spectra were subjected to component analysis as described by Döpner et al.[46]

2.6. Protein-SAM cross-linking. Covalent binding of Lys surface residues to the carboxyl groups of the SAMs was performed according to Ly and co-workers.[47] SAM-coated electrodes were first incubated for 2 hs in solutions containing CMC (20 mg/10 mL) and NHS (6 mg/10 mL), followed by overnight incubation in 10 mM protein solutions. Afterwards, electrodes were immersed in 3 M KCl solutions for 10 min. and thoroughly rinsed with buffer to eliminate non-covalently bound species.

3. RESULTS AND DISCUSSION

This work aims to establish whether ET parameters of Cyt c are correlated with those that characterize the transition to the alternative alkaline conformation. To that end we introduced conservative perturbations at different levels of the protein structure, to assess how these modifications impact on both reactions. Specifically, we studied WT equine Cyt c (Figure 1A),

the mutants Y67F and E66Q, and the WT protein nitrated at the Tyr74 residue (NO_2-Cyt c). Some aspects of these proteins have already been described.[11,12,23,27,35] All these variants have a conserved Met/His axial coordination characteristic of a well folded protein, as verified by Raman (RR) and UV-vis absorption (Figure S1).[12,35] The mutant Y67F was selected because Tyr67 is H-bonded to the axial ligand Met80 in native Cyt c[35] and was identified as crucial for determining protein dynamics.[48–50] Thus, the mutation Y67F interrupts this H-bonding interaction and affects both the pK_a of the alkaline transition[51] and the reorganization energy of the ET reaction.[35] The neighboring Glu66 is implicated in a H-bonding network that connects Met80 with Tyr74, thereby influencing the dynamics of the flexible Ω-loop 70-85.[11] Its replacement was found to affect pK_a.[52] Finally, nitration of Tyr74 leads to deprotonation of this residue at physiological pH, which results in a large pK_a downshift for the alkaline transition.[11,12,27]

To gain some insight into the dynamical behavior of the different proteins, we performed molecular dynamics (MD) simulations. The results do not reveal significant changes of secondary structure composition among variants, but predict differences of flexibility in some specific regions. As shown in Figure 1B, per residue root mean square fluctuations (RMSf) of C_α positions are sensitive to mutations and nitration, particularly at the level of the Ω-loops 20-35, 40-57 and 70-85. The different modifications, however, affect the flexibility of each loop to different extents, such that for the loop 20-35 the average RMSf increases in the order E66Q < Y67F < WT Cyt c < NO_2-Cyt c. For loops 40-57 and 70-85 this order changes to E66Q < WT Cyt c < NO_2-Cyt c < Y67F and NO_2-Cyt c < E66Q < WT cyt c < Y67F, respectively (Table S1).

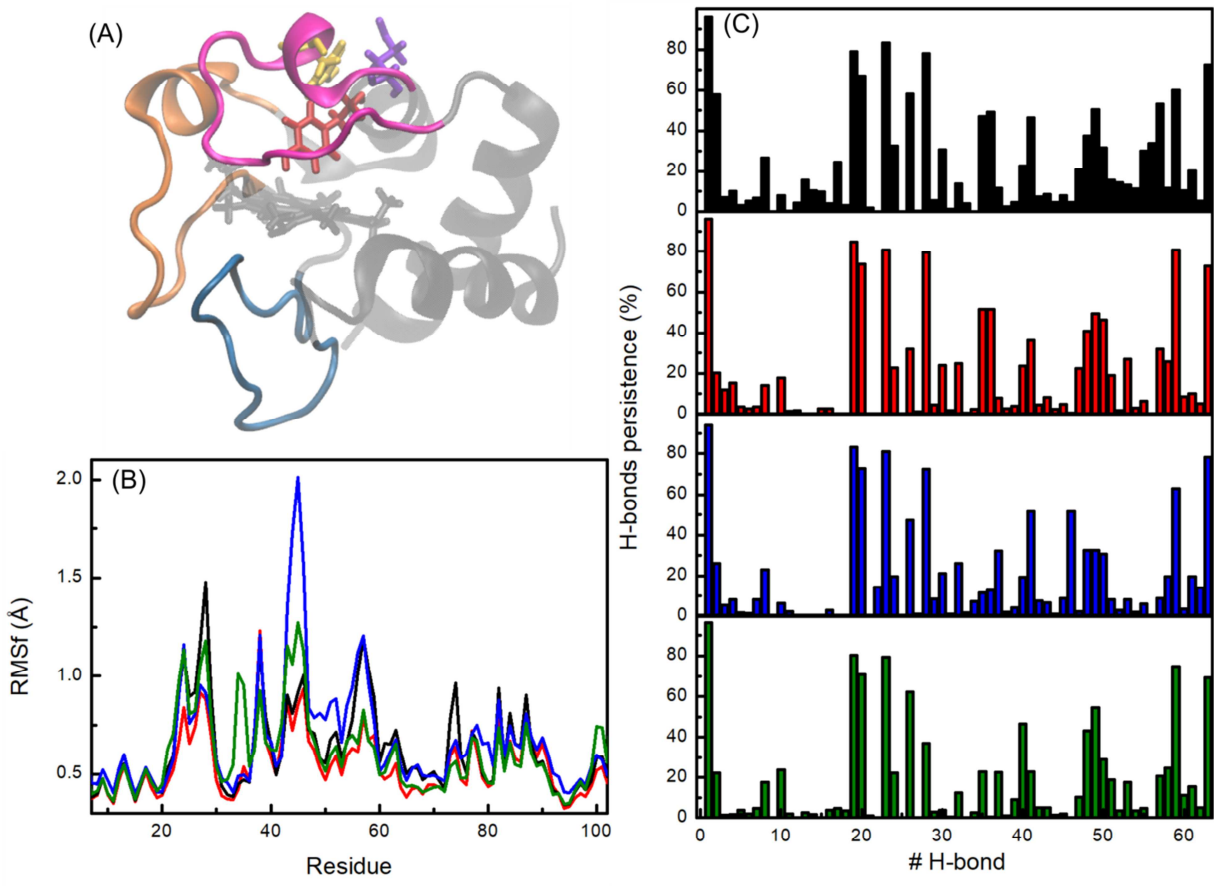

Figure 1. (A) Ferric Cyt c (PDB 1HRC) showing the Ω-loops 20-35 (blue), 40-57 (orange) and 70-85 (pink), and residues Tyr 67 (red), Glu 66 (violet) and Tyr74 (yellow). (B). Per residue RMSf of WT Cyt c (black), E66Q (red), Y67F (blue) and NO_2-Cyt c (green). (C) Percentage of total simulation time that each of the 63 H-bonds belonging to the Ω-loops of WT Cyt c (black), E66Q (red), Y67F (blue) and NO_2-Cyt c (green) remain formed. The donor and acceptor groups of each H-bond are specified in Table S2.

As these perturbations are likely to affect the H-bonding network, we evaluated the persistence of the 63 H-bond interactions identified at the level of the three Ω-loops by computing the fraction of total simulation time that each specific H-bond remains formed. The results summarized in Table S2 and in Figure 1C show that each protein variant is characterized by a distinct pattern of H-bond persistence at the level of the flexible Ω-loops.

3.1. Protein flexibility fine-tunes reduction potentials. The reduction potentials of the proteins in neutral solutions were determined by cyclic voltammetry (CV). For all Cyt c variants the CVs exhibited the typical features of quasi-reversible diffusion-controlled redox reactions (Figure S2), from where E°´ values were estimated as the average of the anodic and cathodic peak positions. The results summarized in Table 1 yield an average E°´ of 267 ± 29 mV. In agreement with the spectroscopic data, this relatively small potential window indicates that the iron coordination is well preserved in all Cyt c variants, as disruption of the labile Fe-Met80 bond at neutral pH is expected to produce E°´ shifts well above 200 mV.[1] Interestingly, E°´ decreases significantly with small increments of the flexibility of either the entire proteins (estimated as the RMSf from residues 7 to 102) or the loop 70-85 (Figure 2A). A similar tendency is observed with the flexibility of the loop 40-57, albeit with larger variations of RMSf, and no clear correlation is observed for the loop 20-35.

Note that an increase of the protein flexibility is likely to imply higher accessibility of the solvent to the redox center. In this scenario one can readily rationalize the observed downshift of E°´, as higher solvent accessibility would result in preferential stabilization of the ferric state.[1] Interestingly, García-Heredia et. al.[14] found that systematic mutation of the Tyr48 residue in a Cyt c from a different organism results in modulation of pK_a and E°´ values, which is paralleled by differences in water accessibility.

Careful inspection of the results summarized in Table S2 shows that out of 63 total H-bonds, the persistence of 4 of them exhibit clear correlations with E°´ (Figure 2B). Three of them belong to the Ω-loop 40-57 (H-bonds 40-57, 48-52 and 55-52) and one is part of the Ω-loop 70-85 (H-bond 70-83), thus pointing out these residues as attractive targets for further mutational studies.

Table 1. Reduction potentials, pKa´s of the alkaline transitions and electron transfer activation energies of the different Cyt c variants. All potentials are reported versus NHE.

	WT Cyt c	E66Q	Y67F	NO_2-Cyt c
[a]E°´(Sn; mV)	263±2	297±7	246±4	265±2
[b]E°´(Ads; mV)	208±2	234±6	196±4	208±5
[c]pK_a(Sn)	9.4±0.1[g]	8.7±0.1	11.0±0.1[h]	7.1±0.1[g]
[d]pK_a(Ads)	10.0±0.3[i]	9.6±0.1	10.5±0.3[i]	8.7±0.1[i]
[e]E_a(C_{16}; kJ mol^{-1})	11.6±0.5	19±5	9.9±0.7[j]	13.5±0.7
[f]E_a(C_6; kJ mol^{-1})	31±2	25±5	33±3	19±0.6
E_F (kJ mol^{-1})	21±3	8±7	23±4	5±2

[a]Determined by CV in solution, pH 7.0. [b]Determined by SERR, adsorbed on C_6-SAMs, pH 7.0. [c]Values from RR titrations in solution. [d]Determined by SERR, adsorbed on C_{11}-SAMs. [e]Determined by TR-SERR, adsorbed on C_{16}-SAMs, pH 7.0. [f]Determined by CV, adsorbed on C_6-SAMs, pH 7.0. [g]From REF[12]. [h]From REF[11]. [i]From REF[27]. [j]From Ref[35].

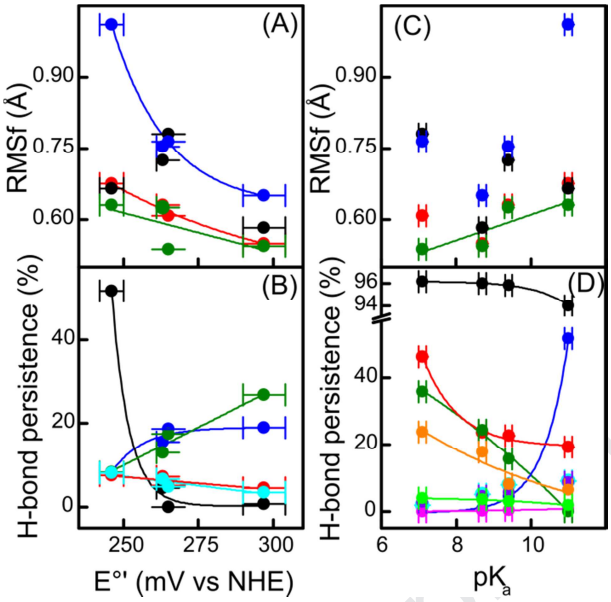

Figure 2. Upper panels: RMSf of the entire protein (red) and of the loops 40-57 (blue), 70-85 (olive) and 20-35 (black) as a function of the E°´(A) and of the pK_a of the alkaline transition (C) of the proteins in solution. Lower panels: Persistence of H-bonds as a function of E°´ (B) and of pK_a (D) of the proteins in solution. The color codes specify residues involved in each H-bond. (C): black 48-43, blue 55-52, red 40-57, cyan 22-104, olive 70-83. (D): black 18-30, blue 48-43, red 40-52, cyan 42-53, magenta 66-74, olive 67-80, violet 35-32, orange 26-24, green 22-33. The lines are included to guide the eye.

It is well established that the interactions of mammalian Cyt c with redox partner proteins are electrostatically driven.[1,53] Moreover, about 15% of the Cyt c molecules present in the intermembrane mitochondrial space are associated with negatively charged partners such as cardiolipin and complexes III and IV.[54] Therefore, in order to assess the possible impact of electrostatic interactions on the redox parameters of Cyt c, we investigated the adsorption of the four variants on negatively charged biomimetic surfaces constructed from self-assembled monolayers (SAMs) of 1:1 mixtures of HS-$(CH_2)_{n-1}$-COOH and HS-$(CH_2)_n$-OH on Au and Ag electrodes. The adsorbed proteins were monitored by SERR as a function of the electrode

potential. In all cases SERR spectra measured at sufficiently positive or negative electrode potentials were indistinguishable from the corresponding RR spectra in solution of the native ferric and ferrous proteins, respectively (Figure S3). These results confirm that for all Cyt c variants the heme structure is well preserved upon adsorption. The E°´ values obtained from deconvolution of the SERR spectra (Figures S4-S7) are summarized in Table 1. In agreement with previous observations,[13,27,35] these values are about 60 mV lower than in solution under, otherwise, identical conditions. These differences can be largely ascribed to the potential drop across the SAMs,[55] but may also reflect subtle deformations that do not affect the iron coordination.[35] Direct electrochemistry of the adsorbed proteins was also probed by CV, yielding E°´ values similar to those obtained by SERR (Figure S8).

Interestingly, the E°´ values of the adsorbed proteins exhibit correlations with the flexibility parameters and H-bond persistence (Figure S9) that are qualitatively similar to those presented in Figures 2A and 2B for the same species in solution.

Previous investigations have demonstrated that Cyt c/SAM interactions involve the same set of positively charged surface residues that constitute the binding site for cytochrome *c* oxidase, cytochrome *c* peroxidase and bc_1 complex, namely lysines 13, 86 and 87, and to a lesser extent lysines 8, 72 and 73.[53] Therefore protein adsorption is not expected to affect the flexibility of the loop 40-57 loop and to affect only to some extent the flexibility of the loop 70-85. This prediction is consistent with the qualitatively similar correlations found for E°´ values of solution and adsorbed species with the RMSf of the Ω loops obtained from simulations carried out in aqueous solution.

3.2. Protein flexibility and the alkaline conformational transition. The pK_a´s for the alkaline transitions of the different proteins in solution were determined by acid-base titrations monitored by UV-vis absorption and by RR spectroscopy (Figures S10-S11).[12,27] The obtained values summarized in Table 1 are in very good agreement with previous reports.[11,12,27] Albeit with some scattering, we observe a systematic increase of pK_a with the RMSf of loop 70-85, but no clear tendencies with the flexibilities of the other two loops (Figure 2C). On the other hand pK_a´s can be correlated with the persistence of 9 of the 63 H-bonds (Figure 2D) distributed throughout the flexible regions of the proteins, including 4 H-bonds belonging to loop 20-35 (H-bonds 18-30, 22-33, 26-24 and 35-32), 3 from loop 40-57 (H-bonds 40-52, 42-53 and 48-43) and 2 with at least one residue from loop 70-85 (H-bonds 66-74 and 67-80). Thus, the thermodynamic parameters of conformational transition and redox reactions (pK_a and E°´, respectively) appear to be dependent on protein dynamics, but each magnitude is fine-tuned by the flexibility of different structural elements (Figure 2).

We also investigated the effect of electrostatic interactions on the alkaline transitions using SAM-coated Ag electrodes. The adsorbed proteins were monitored by SERR spectroscopy as a function of the solution pH and of the electrode potential. In all cases SERR spectra recorded at open circuit or at electrode potentials above E°´could be quantitatively simulated with only two spectral components that are identical to the RR spectra of ferric native and alkaline conformations in solution (Figures S12), thereby indicating that the alkaline conformations obtained in solution and in electrostatic complexes are identical regarding the characteristic Lys/His axial coordination. Upon application of potentials well below E°´ the SERR spectra present a single component identical to the RR spectra of the native proteins in neutral solution, thus confirming that in the ferrous state conformational equilibria are completely displaced

towards the Met/His native form. In agreement with previous observations,[27] pK_a values obtained for the adsorbed proteins are shifted by 0.6-1.6 units with respect to solution (Table 1). In spite of these shifts, the pK_a´s of the adsorbed proteins exhibit correlations with the persistence of the same 9 H-bonds and with the RMSf of loop 70-85 (Figure S9) that are qualitatively similar to those shown in Figure 2 for solution pK_a´s. These results suggest that the reaction in electrostatic complexes is influenced by the same dynamical features than in solution.

The minimal reaction mechanism of the alkaline transition consists of a first (pre-equilibrium) deprotonation step regarded as the triggering event, followed by a reversible Met-Lys axial ligand exchange step[26,27] (reaction 1):

$$\mathrm{Met/His^{3+}_{protonated}} \overset{K_H}{\rightleftharpoons} \mathrm{Met/His^{3+}_{deprotonated}} \underset{k_b}{\overset{k_f}{\rightleftharpoons}} \mathrm{Lys/His^{3+}} \qquad \text{(Reaction 1)}$$

$$\mathrm{Met/His^{2+}} \underset{k_2}{\overset{k_1}{\rightleftharpoons}} \mathrm{Met/His^{3+}} \underset{k_4}{\overset{k_3}{\rightleftharpoons}} \mathrm{Lys/His^{3+}} \qquad \text{(Reaction 2)}$$

This mechanism leads to the expression $pK_a = pK_H + \log(k_b/k_f)$. The nature of the triggering event is a matter of debate but most likely it corresponds to a collective process involving deprotonation and H-bonding rearrangement of several amino acids, rather than deprotonation of a single residue.[24] The facts that H-bonding dynamics differs among Cyt c variants (Figure 1C), and that pK_a´s correlate with the persistence of an extended H-bond network (Figures 2D and S9) suggest that pK_a´s are mainly determined by the corresponding pK_H´s. To verify this hypothesis we investigated the dynamics of the transitions by time-resolved SERR (TR-SERR).[27] In these experiments the proteins adsorbed on SAM-coated electrodes are initially subjected to sufficiently low potentials to stabilize the native ferrous conformation. The system is

then perturbed with a positive potential jump to trigger fast oxidation and the subsequent Met-Lys ligand exchange of the ferric protein (Reaction 2). The constants in reactions 1 and 2 can be related as $k_3 = K_H k_f/(K_H+[H^+])$, thus implying that K_H can be obtained from the pH-dependence of k_3. The progress of the reaction is monitored by acquiring SERR spectra at various delay times after the perturbation. The obtained TR-SERR spectra could be quantitatively simulated using three spectral components that correspond to the ferrous and ferric Met/His native conformation and the ferric Lys/His alkaline form (Figures 3A and S13), yielding concentration profiles as those shown in Figures 3B and S13. The dependencies of k_3 with pH are shown in Figure 3C. Except for NO_2-Cyt c, the inflexion points of the sigmoidal curves, which correspond to K_H, are outside the experimentally accessible pH window, thus hampering reliable determinations. From the shapes of the curves, however, one can safely conclude that K_H values increase in the order NO_2-Cyt c < E66Q < WT Cyt c < Y67F , i.e. similar to the order of the pK_a´s. On the other hand, the fact that pK_a increases with the flexibility of the loop 70-85 suggests that the different mutations and chemical modifications might affect k_f and k_b to different extents, thus making the contribution of $\log(k_b/k_f)$ not negligible, albeit detail kinetic studies to determine k_b and k_f are far from trivial and beyond the scope of the present work.

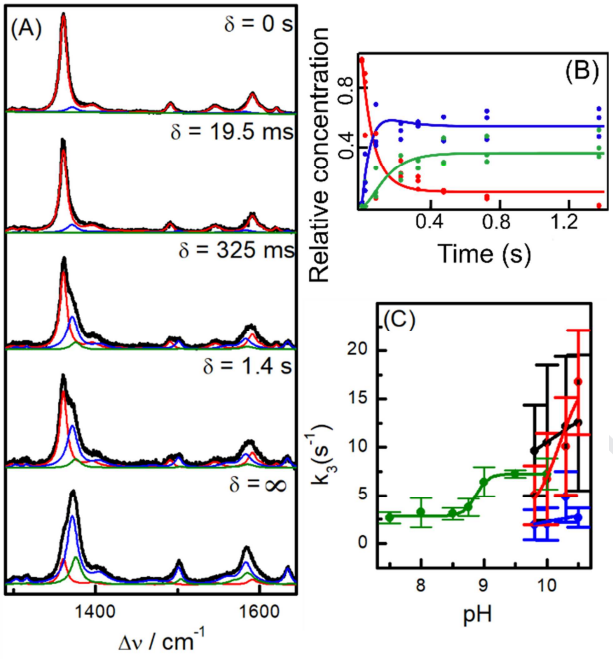

Figure 3. (A) TR-SERR spectra of E66Q adsorbed on a C_{11}-SAM measured at different delay times after applying a potential jump that triggers the redox-linked alkaline transition. Black: experimental spectra. Red: ferrous native spectral component. Blue: ferric native spectral component. Green: ferric alkaline spectral component. (B) Concentration profile obtained from quantitative deconvolution of the TR-SERR spectra shown in panel (A). The lines are obtained by global fitting according to reaction 2. Pannels (A) and (B) share the same color code. (C) Variation of k_3 with pH for the different Cyt c variants. Black: WT Cyt-c. Red: E66Q. Blue: Y67F. Green: NO_2-Cyt c. The lines are included to guide the eye.

3.3. Protein flexibility and electron transfer dynamics. To determine how the different structural modifications of Cyt c affect ET kinetics, we performed electrochemical and spectroelectrochemical kinetic experiments at neutral pH of protein samples adsorbed on Au and Ag SAM-coated electrodes of variable thickness (n = 4, 6, 8, 11 and 16). For thick SAMs, where heterogeneous ET is sufficiently slow, ET rate constants (k_{ET}) were determined by TR-SERR following established procedures[55] (Figures S14-S16). In addition k_{ET} values were determined by CV using Laviron´s method[56] for all SAM thicknesses (Figure S17-S19). In agreement with

previous reports,[1] k_{ET} values obtained for the thicker SAMs (n > 8) decrease exponentially with distance at a decay rate of ~ 0.9 per CH_2 group, which is consistent with a nonadiabatic ET mechanism. For the thinner films (n < 8) the distance dependence is significantly softer and actually k_{ET} tends to a plateau upon shortening the SAM length (Figure S20). The onset of this plateau might originate in a reorientation step becoming rate limiting with increasing electronic couplings.[57] To check this hypothesis we fixed the orientation of the immobilized proteins by cross-linking surface lysine residues of pre-adsorbed protein samples to carboxyl groups of the SAMs. The distance-dependencies of k_{ET} obtained for the covalently attached proteins are essentially identical to those obtained for electrostatic adsorption (Figure S20), thus indicating that protein reorientation is not rate determining under the present conditions. As additional control experiments, we measured potential-dependent SERR spectra of the adsorbed proteins using Q-band excitation. Under these conditions the intensity ratio of vibrational modes of different symmetry, such as B_{1g} versus A_{1g} modes, are sensitive to the average protein orientation in the electrostatic complexes.[57] We observe slopes that vary between 0.027 and 0.04 mV^{-1} for the different protein variants and modes of immobilization (Figures S21-S23), which within experimental error, can be regarded as a relatively small variation. Moreover, the proximity of the slopes obtained for chemisorbed and physisorbed samples strongly suggests that large amplitude potential-dependent reorientation can be safely discarded.

Alternatively, the distance-dependence of k_{ET} can be rationalized in terms of a change of ET mechanism. At the thicker SAMs the electronic coupling is sufficiently small so that the reaction can be treated in terms of Marcus semiclassical expression for electrochemical ET at metal electrodes.[58,59] In this regime k_{ET} decays exponentially with the electronic coupling and is independent of the medium viscosity (η). Deviations from the exponential distance decay and

deceleration of k_{ET} with η are indicative of entering the friction control regime, typically at the thinner SAMs.[45,60,61] Indeed, all the proteins studied here exhibit a strong decay of k_{ET} with η within the physiological range from 1 to 40 cP, which was adjusted by addition of sucrose or polyethylene glycol (Figures 4A and S24-S25). The decay of k_{ET} with η follows a power law of the form $k_{ET} \propto \eta^{-\gamma}$. Within experimental error, the parameter γ is the same for adsorbed and cross-linked proteins, thus further confirming that ET is not rate limited by large amplitude protein reorientation. Moreover, γ increases with electronic coupling, thus suggesting a gradual transition from nonadiabatic to friction-controlled ET (Figure 4B). Control experiments show that E°′, as well as the SERR spectra of the different proteins recorded with Soret- and Q-band excitation remain unchanged upon addition of the thickening agent (Figures S26-S27).

In a next step we determined the activation energies of the heterogeneous ET reactions at two different SAM thicknesses, n = 6 and n = 16, using two independent methods: (i) by CV from the temperature dependence of k_{ET} at zero driving force (Figure S18) and (ii) from the driving force (overpotential) dependence of k_{ET} at constant temperature by TR-SERR (Figures S14-S16). As summarized in Table 1, activation energies obtained at the thicker SAMs, $E_a(C_{16})$, for WT Cyt c, Y67F and NO_2-Cyt c are significantly lower than those obtained at the thinner SAMs, $E_a(C_6)$. Consistently, we observe the same tendency for E66Q, albeit in this case the difference is closer to the standard deviation of the measurements. Interestingly, $E_a(C_{16})$ is strongly dependent on the same flexibility parameters that modulate E°′ (compare Figures 5 and 2), i.e. the RMSf of loops 40-57 and 70-85 and the persistence of H-bonds 48-43, 55-52, 40-57, 22-104 and 70-83. $E_a(C_6)$, in contrast, correlates with the same flexibility parameters that modulate the pK_a′s of the alkaline transitions (compare Figures 5 and 2), i.e. with the RMSf of loop 70-85 and with the persistence of H-bonds 18-30, 48-43, 40-52, 42-53, 66-74, 67-80, 35-32, 26-24 and 22-33.

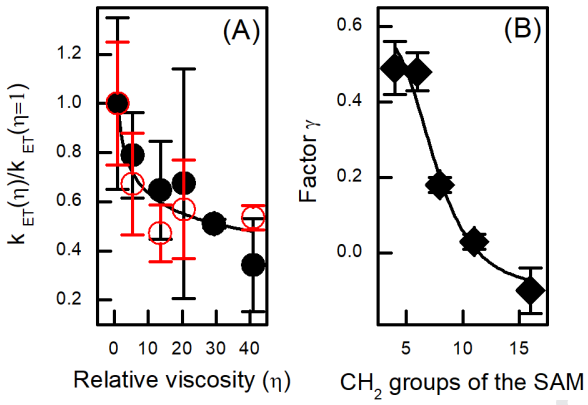

Figure 4. (A) Normalized ET rate constants of WT Cyt c adsorbed (black) and cross-linked (red) to a C_6-SAM, as a function of the solution viscosity adjusted by addition of PEG. The line is a fitting to the empirical expression $k_{ET}(\eta)/k_{ET}(\eta=1) = \eta^{-\gamma}$. (B) Variation of the parameter γ obtained for WT Cyt c, as a function of the SAM thickness.

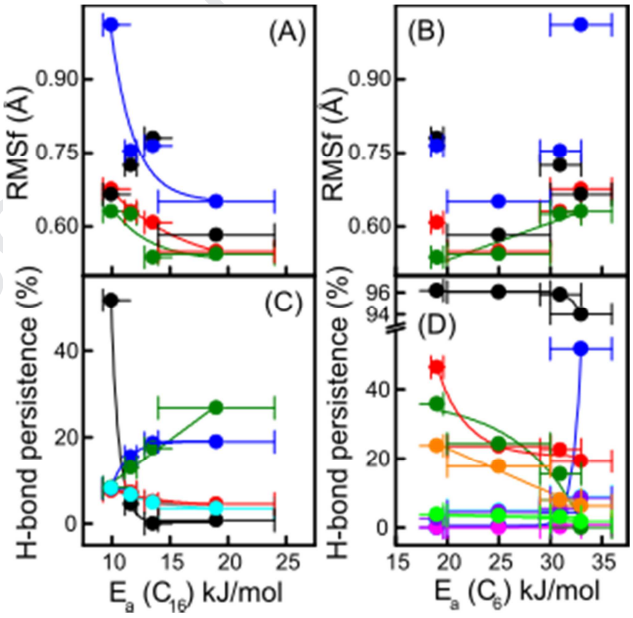

Figure 5. Upper panels: RMSf of the entire protein (red) and of the loops 40-57 (blue), 70-85 (olive) and 20-35 (black) as a function of ET activation energies measured on C_{16}-SAMs (A) and C_6-SAMs (B). Lower panels: persistence of H-bonds as a function of ET activation energies

measured on C_{16}-SAMs (C) and C_6-SAMs (D). The color codes specify residues involved in each H-bond. (C): black 48-43, blue 55-52, red 40-57, cyan 22-104, olive 70-83. (D): black 18-30, blue 48-43, red 40-52, cyan 42-53, magenta 66-74, olive 67-80, violet 35-32, orange 26-24, green 22-33. The lines are included to guide the eye.

Two different theoretical models have been recently applied to account for distance-dependencies of the ET activation energies upon entering the frictional regime.[60,62,63] The two models differ in very fundamental aspects but, for small temperature ranges and assuming ergodicity, both lead to an Arrhenius-like expression for k_{ET} at zero driving force, where the measured activation energy can be expressed as $E_a = \lambda/4 + E_F$. Here λ is Marcus ET reorganization energy, while E_F is a term that accounts for the activation energy of the frictionally controlled component of the reaction, which can be associated to protein/SAM conformational oscillations. In the nonadiabatic regime the measured E_a is expected to reflect Marcus reorganization energy only, while values determined at short tunneling distances contain both contributions. Therefore, the difference between values determined at C_6- and C_{16}-SAMs affords a good estimation of the frictional component $E_F = E_a(C_6)-E_a(C_{16})$. As shown in Table 1 E_F is not negligible as it accounts for 25 to 70 % of $E_a(C_6)$, depending on the protein variant. In terms of Matyushov´s model[63] E_F reports on the T-dependence of relatively slow protein/SAM oscillations. Therefore, E_F and $E_a(C_6)$ can be anticipated to be strongly dependent on the flexibility of the SAM/protein linker, i.e. on the RMSf of loop 70-85 that contains most of the residues that constitute the binding site.[53] The data in Figure 5B are in good agreement with this interpretation. λ, in contrast, is related to the inner sphere reorganization of the metal site

(λ_{in}) and to the polarization response of the protein matrix and solvent (λ_{out}) in a much shorter time scale. Most likely, the decrease of λ with increasing protein flexibility (Figure 5C) is related to a decrease of the λ_{out} component rather than to variations of λ_{in}.

4. CONCLUSIONS

The present results reveal that thermodynamic and kinetic parameters that characterize the canonical electron transport function of Cyt c and the transition to alternative conformations that eventually lead to a gain of new functions are all strongly modulated by protein flexibility. Different parameters, however, are particularly responsive to the dynamics of distinct structural elements. Reduction potentials and long-range ET reorganization energies are correlated (Figure 6A) as both are strongly dependent on the water accessibility to the metal redox site, which in turn is mainly determined by the flexibility of the Ω-loops 40-57 and 70-85.

On the other hand, pK_a values of the alkaline transition correlate with the activation energies of frictionally-controlled ET (Figure 6B) as both parameters are mainly modulated by the flexibility of the Ω-loop 70-85. This latter loop appears to be decisive for defining Cyt c function. Its flexibility tends to stabilize a Cyt c native form of low λ at the same time that pushes pK_a to unphysiologically high values, thus favoring the canonical electron shuttling function. Pro-apoptotic stimuli raise intra-mitochondrial viscosity, thus bringing the system into an unfavourable friction control ET regime of high activation energy that may hamper the respiratory function. These findings are in agreement with previous investigations by the Englander group[26,64] that showed continuous unfolding/refolding dynamics of the Ω-loop foldons 40-57 and 70-85, which in turn crucially define the alkaline transition. Moreover, mutational investigations of Cyt c from other organisms have determined that mutations at the

level of the Ω-loop 40-57 may alter either $E°'$ or pK_a,[16,21,25] albeit the available information is insufficient for establishing correlations, particularly with regard to kinetic ET parameters.

Interestingly, aside of their distinct dependencies on specific dynamical features, all the measured thermodynamic and kinetic parameters vary systematically, albeit with some scattering, with the persistence of a single H-bonding interaction between the first and second coordination sphere ligands Met80 and Tyr67 (Figure 6C). Moreover, while the Y67F mutation upshifts the pK_a by 1.6 units and nitration of Tyr74 from WT Cyt c results in a 2.3 units downshift, nitration of Y67F at the same position has no significant effect on the pK_a (Figure S28), thereby highlighting the critical role of the highly conserved Tyr67, its polarity and its interaction with Met 80, which are both affected upon Y67F mutation.[35,48–50]

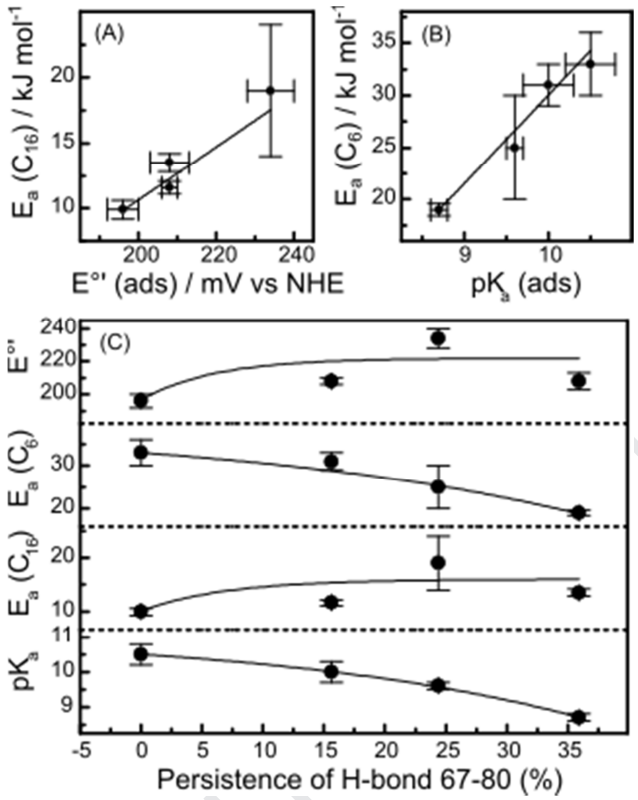

Figure 6. (A) and (B): variation of the ET activation energies measured at C16-SAMs and C6-SAMs with the reduction potentials and pKa´s, respectively. (C): Variation of the different thermodynamic and kinetic parameters with the persistence of the H-bond 67-80 expressed as percentage of the total simulation time that remains formed.

SUPLEMENTARY DATA

Supplementary data to this article can be found online.

NOTES

The authors declare no competing interest

ACKNOWLEDGMENT

This work was supported by ANPCyT, CONICET and UBA, Argentina, and by ANII and UdelaR, Uruguay.

REFERENCES

[1] D. Alvarez-Paggi, L. Hannibal, M.A. Castro, S. Oviedo-Rouco, V. Demicheli, V. Tórtora, F. Tomasina, R. Radi, D.H. Murgida, Multifunctional Cytochrome c: Learning New Tricks from an Old Dog, Chem. Rev. 117 (2017) 13382–13460. https://doi.org/10.1021/acs.chemrev.7b00257.

[2] M. Imai, T. Saio, H. Kumeta, T. Uchida, F. Inagaki, K. Ishimori, Investigation of the redox-dependent modulation of structure and dynamics in human cytochrome c, Biochem. Biophys. Res. Commun. 469 (2016) 978–984. https://doi.org/10.1016/j.bbrc.2015.12.079.

[3] G.W. Bushnell, G.V. Louie, G.D. Brayer, High-resolution three-dimensional structure of horse heart cytochrome c, J. Mol. Biol. 214 (1990) 585–595. https://doi.org/10.1016/0022-2836(90)90200-6.

[4] L. Hannibal, F. Tomasina, D.A. Capdevila, V. Demicheli, V. Tórtora, D. Alvarez-Paggi, R. Jemmerson, D.H. Murgida, R. Radi, Alternative Conformations of Cytochrome c: Structure, Function, and Detection, Biochemistry. 55 (2016) 407–428. https://doi.org/10.1021/acs.biochem.5b01385.

[5] S. Orrenius, B. Zhivotovsky, Cardiolipin oxidation sets cytochrome *c* free, Nat. Chem. Biol. 1 (2005) 188–189. https://doi.org/10.1038/nchembio0905-188.

[6] S. Yuan, C.W. Akey, Apoptosome Structure, Assembly, and Procaspase Activation, Structure. 21 (2013) 501–515. https://doi.org/10.1016/j.str.2013.02.024.

[7] J. Martínez-Fábregas, I. Díaz-Moreno, K. González-Arzola, S. Janocha, J.A. Navarro, M. Hervás, R. Bernhardt, A. Velázquez-Campoy, A. Díaz-Quintana, M.A.D. la Rosa, Structural and Functional Analysis of Novel Human Cytochrome c Targets in Apoptosis, Mol. Cell. Proteomics. 13 (2014) 1439–1456. https://doi.org/10.1074/mcp.M113.034322.

[8] R. Santucci, F. Sinibaldi, P. Cozza, F. Polticelli, L. Fiorucci, Cytochrome c: An extreme multifunctional protein with a key role in cell fate, Int. J. Biol. Macromol. 136 (2019) 1237–1246. https://doi.org/10.1016/j.ijbiomac.2019.06.180.

[9] S.C. Kim, R. Sprung, Y. Chen, Y. Xu, H. Ball, J. Pei, T. Cheng, Y. Kho, H. Xiao, L. Xiao, N.V. Grishin, M. White, X.-J. Yang, Y. Zhao, Substrate and Functional Diversity of Lysine Acetylation Revealed by a Proteomics Survey, Mol. Cell. 23 (2006) 607–618. https://doi.org/10.1016/j.molcel.2006.06.026.

[10] J.M. García-Heredia, I. Díaz-Moreno, A. Díaz-Quintana, M. Orzáez, J.A. Navarro, M. Hervás, M.A. De la Rosa, Specific nitration of tyrosines 46 and 48 makes cytochrome c assemble a non-functional apoptosome, FEBS Lett. 586 (2012) 154–158. https://doi.org/10.1016/j.febslet.2011.12.007.

[11] L.A. Abriata, A. Cassina, V. Tórtora, M. Marín, J.M. Souza, L. Castro, A.J. Vila, R. Radi, Nitration of Solvent-exposed Tyrosine 74 on Cytochrome c Triggers Heme Iron-Methionine 80 Bond Disruption. Nuclear Magnetic Resonance and Optical Spectroscopy Studies, J. Biol. Chem. 284 (2009) 17–26. https://doi.org/10.1074/jbc.M807203200.

[12] D.A. Capdevila, D. Álvarez-Paggi, M.A. Castro, V. Tórtora, V. Demicheli, D.A. Estrín, R. Radi, D.H. Murgida, Coupling of tyrosine deprotonation and axial ligand exchange in nitrocytochrome c, Chem. Commun. 50 (2014) 2592–2594. https://doi.org/10.1039/C3CC47207H.

[13] D.A. Capdevila, W.A. Marmisollé, F. Tomasina, V. Demicheli, M. Portela, R. Radi, D.H. Murgida, Specific methionine oxidation of cytochrome c in complexes with zwitterionic

lipids by hydrogen peroxide: Potential implications for apoptosis, Chem. Sci. 6 (2015) 705–713. https://doi.org/10.1039/c4sc02181a.

[14] J.M. García-Heredia, A. Díaz-Quintana, M. Salzano, M. Orzáez, E. Pérez-Payá, M. Teixeira, M.A. De la Rosa, I. Díaz-Moreno, Tyrosine phosphorylation turns alkaline transition into a biologically relevant process and makes human cytochrome c behave as an anti-apoptotic switch, J. Biol. Inorg. Chem. 16 (2011) 1155–1168. https://doi.org/10.1007/s00775-011-0804-9.

[15] J. Wan, H.A. Kalpage, A. Vaishnav, J. Liu, I. Lee, G. Mahapatra, A.A. Turner, M.P. Zurek, Q. Ji, C.T. Moraes, M.-A. Recanati, L.I. Grossman, A.R. Salomon, B.F.P. Edwards, M. Hüttemann, Regulation of Respiration and Apoptosis by Cytochrome c Threonine 58 Phosphorylation, Sci. Rep. 9 (2019) 1–16. https://doi.org/10.1038/s41598-019-52101-z.

[16] B. Moreno-Beltrán, A. Guerra-Castellano, A. Díaz-Quintana, R.D. Conte, S.M. García-Mauriño, S. Díaz-Moreno, K. González-Arzola, C. Santos-Ocaña, A. Velázquez-Campoy, M.A.D. la Rosa, P. Turano, I. Díaz-Moreno, Structural basis of mitochondrial dysfunction in response to cytochrome c phosphorylation at tyrosine 48, Proc. Natl. Acad. Sci. 114 (2017) E3041–E3050. https://doi.org/10.1073/pnas.1618008114.

[17] I. Lee, A.R. Salomon, K. Yu, J.W. Doan, L.I. Grossman, M. Hüttemann, New Prospects for an Old Enzyme: Mammalian Cytochrome c Is Tyrosine-Phosphorylated in Vivo, Biochemistry. 45 (2006) 9121–9128. https://doi.org/10.1021/bi060585v.

[18] H. Yu, I. Lee, A.R. Salomon, K. Yu, M. Hüttemann, Mammalian liver cytochrome c is tyrosine-48 phosphorylated in vivo, inhibiting mitochondrial respiration, Biochim. Biophys. Acta BBA - Bioenerg. 1777 (2008) 1066–1071. https://doi.org/10.1016/j.bbabio.2008.04.023.

[19] G. Mahapatra, A. Varughese, Q. Ji, I. Lee, J. Liu, A. Vaishnav, C. Sinkler, A.A. Kapralov, C.T. Moraes, T.H. Sanderson, T.L. Stemmler, L.I. Grossman, V.E. Kagan, J.S. Brunzelle, A.R. Salomon, B.F.P. Edwards, M. Hüttemann, Phosphorylation of Cytochrome c Threonine 28 Regulates Electron Transport Chain Activity in Kidney: Implications for AMP Kinase, J. Biol. Chem. (2016) jbc.M116.744664. https://doi.org/10.1074/jbc.M116.744664.

[20] H.A. Kalpage, A. Vaishnav, J. Liu, A. Varughese, J. Wan, A.A. Turner, Q. Ji, M.P. Zurek, A.A. Kapralov, V.E. Kagan, J.S. Brunzelle, M.-A. Recanati, L.I. Grossman, T.H. Sanderson, I. Lee, A.R. Salomon, B.F.P. Edwards, M. Hüttemann, Serine-47 phosphorylation of cytochrome c in the mammalian brain regulates cytochrome c oxidase and caspase-3 activity, FASEB J. 33 (2019) 13503–13514. https://doi.org/10.1096/fj.201901120R.

[21] P. Pecina, G.G. Borisenko, N.A. Belikova, Y.Y. Tyurina, A. Pecinova, I. Lee, A.K. Samhan-Arias, K. Przyklenk, V.E. Kagan, M. Hüttemann, Phosphomimetic Substitution of Cytochrome c Tyrosine 48 Decreases Respiration and Binding to Cardiolipin and Abolishes Ability to Trigger Downstream Caspase Activation, Biochemistry. 49 (2010) 6705–6714. https://doi.org/10.1021/bi100486s.

[22] V.E. Kagan, H.A. Bayır, N.A. Belikova, O. Kapralov, Y.Y. Tyurina, V.A. Tyurin, J. Jiang, D.A. Stoyanovsky, P. Wipf, P.M. Kochanek, J.S. Greenberger, B. Pitt, A.A. Shvedova, G. Borisenko, Cytochrome c/cardiolipin relations in mitochondria: a kiss of death, Free Radic. Biol. Med. 46 (2009) 1439–1453. https://doi.org/10.1016/j.freeradbiomed.2009.03.004.

[23] D.A. Capdevila, R. Oviedo, F. Tomasina, V. Tortora, V. Demicheli, R. Radi, D.H. Murgida, Active Site Structure and Peroxidase Activity of Oxidatively Modified

Cytochrome c Species in Complexes with Cardiolipin, Biochemistry. 54 (2015) 7491–7504. https://doi.org/10.1021/acs.biochem.5b00922.
[24] O.M. Deacon, D.A. Svistunenko, G.R. Moore, M.T. Wilson, J.A.R. Worrall, Naturally Occurring Disease-Related Mutations in the 40–57 Ω-Loop of Human Cytochrome c Control Triggering of the Alkaline Isomerization, Biochemistry. 57 (2018) 4276–4288. https://doi.org/10.1021/acs.biochem.8b00520.
[25] O.M. Deacon, R.W. White, G.R. Moore, M.T. Wilson, J.A.R. Worrall, Comparison of the structural dynamic and mitochondrial electron-transfer properties of the proapoptotic human cytochrome c variants, G41S, Y48H and A51V, J. Inorg. Biochem. 203 (2020) 110924. https://doi.org/10.1016/j.jinorgbio.2019.110924.
[26] L. Hoang, H. Maity, M.M.G. Krishna, Y. Lin, S.W. Englander, Folding Units Govern the Cytochrome c Alkaline Transition, J. Mol. Biol. 331 (2003) 37–43. https://doi.org/10.1016/S0022-2836(03)00698-3.
[27] S. Oviedo-Rouco, M.A. Castro, D. Alvarez-Paggi, C. Spedalieri, V. Tortora, F. Tomasina, R. Radi, D.H. Murgida, The alkaline transition of cytochrome c revisited: Effects of electrostatic interactions and tyrosine nitration on the reaction dynamics, Arch. Biochem. Biophys. 665 (2019) 96–106. https://doi.org/10.1016/j.abb.2019.02.016.
[28] B. De, D.A. Paggi, F. Doctorovich, P. Hildebrandt, D.A. Estrin, D.H. Murgida, M.A. Marti, Molecular basis for the electric field modulation of cytochrome c structure and function, J. Am. Chem. Soc. 131 (2009) 16248–16256. https://doi.org/10.1021/ja906726n.
[29] M.M. Cherney, B.E. Bowler, Protein dynamics and function: Making new strides with an old warhorse, the alkaline conformational transition of cytochrome c, Coord. Chem. Rev. 255 (2011) 664–677. https://doi.org/10.1016/j.ccr.2010.09.014.
[30] D. De Rocco, C. Cerqua, P. Goffrini, G. Russo, A. Pastore, F. Meloni, E. Nicchia, C.T. Moraes, A. Pecci, L. Salviati, A. Savoia, Mutations of cytochrome c identified in patients with thrombocytopenia THC4 affect both apoptosis and cellular bioenergetics, Biochim. Biophys. Acta BBA - Mol. Basis Dis. 1842 (2014) 269–274. https://doi.org/10.1016/j.bbadis.2013.12.002.
[31] M.D. Liptak, R.D. Fagerlund, E.C. Ledgerwood, S.M. Wilbanks, K.L. Bren, The Proapoptotic G41S Mutation to Human Cytochrome c Alters the Heme Electronic Structure and Increases the Electron Self-Exchange Rate, J. Am. Chem. Soc. 133 (2011) 1153–1155. https://doi.org/10.1021/ja106328k.
[32] V. Rodríguez-Roldán, J.M. García-Heredia, J.A. Navarro, M.A.D. la Rosa, M. Hervás, Effect of Nitration on the Physicochemical and Kinetic Features of Wild-Type and Monotyrosine Mutants of Human Respiratory Cytochrome c, Biochemistry. 47 (2008) 12371–12379. https://doi.org/10.1021/bi801329s.
[33] G. Battistuzzi, M. Borsari, M. Sola, Redox Properties of Cytochrome c, Antioxid. Redox Signal. 3 (2001) 279–291. https://doi.org/10.1089/152308601300185232.
[34] J.R. Winkler, H.B. Gray, Electron flow through metalloproteins, Chem. Rev. 114 (2014) 3369–3380. https://doi.org/10.1021/cr4004715.
[35] D. Alvarez-Paggi, M.A. Castro, V. Tórtora, L. Castro, R. Radi, D.H. Murgida, Electrostatically driven second-sphere ligand switch between high and low reorganization energy forms of native cytochrome c, J. Am. Chem. Soc. 135 (2013) 4389–4397. https://doi.org/10.1021/ja311786b.
[36] L. Milazzo, L. Tognaccini, B.D. Howes, G. Smulevich, Probing the non-native states of Cytochrome c with resonance Raman spectroscopy: A tool for investigating the structure–

function relationship, J. Raman Spectrosc. 49 (2018) 1041–1055. https://doi.org/10.1002/jrs.5315.
[37] P. Weinkam, J. Zimmermann, F.E. Romesberg, P.G. Wolynes, The Folding Energy Landscape and Free Energy Excitations of Cytochrome c, Acc. Chem. Res. 43 (2010) 652–660. https://doi.org/10.1021/ar9002703.
[38] S. Zaidi, M.I. Hassan, A. Islam, F. Ahmad, The role of key residues in structure, function, and stability of cytochrome c, Cell. Mol. Life Sci. 71 (2014) 229–255. https://doi.org/10.1007/s00018-013-1341-1.
[39] C. Batthyány, J.M. Souza, R. Durán, A. Cassina, C. Cerveñansky, R. Radi, Time Course and Site(s) of Cytochrome *c* Tyrosine Nitration by Peroxynitrite †, Biochemistry. 44 (2005) 8038–8046. https://doi.org/10.1021/bi0474620.
[40] G.W. Bushnell, G.V. Louvie, G.D. Brayer, High-resolution three-dimensional structure of horse heart cytochrome c., J Mol Biol. 214 (1990) 585–595.
[41] H.J.C. Berendsen, J.P.M. Postma, W.F. van Gunsteren, J.R. Haak, Molecular dynamics with coupling to an external bath, J Chem Phys. 81 (1984) 3984.
[42] D.A. Case, R.M. Betz, D.S. Cerutti, T.E. Cheatham, III, T.A. Darden, R.E. Duke, T.J. Giese, H. Gohlke, A.W. Goetz, N. Homeyer, S. Izadi, P. Janowski, J. Kaus, A. Kovalenko, T.S. Lee, S. LeGrand, P. Li, C. Lin, T. Luchko, R. Luo, B. Madej, D. Mermelstein, K.M. Merz, G. Monard, H. Nguyen, H.T. Nguyen, I. Omelyan, A. Onufriev, D.R. Roe, A. Roitberg, C. Sagui, C.L. Simmerling, W.M. Botello-Smith, J. Swails, R.C. Walker, J. Wang, R.M. Wolf, X. Wu, L. Xiao and P.A. Kollman (2016), AMBER 2016, University of California, San Francisco.
[43] J.A. Maier, C. Martínez, K. Casavajhala, L. Wickstrom, K.E. Hauser, C. Simmerling, ff14SB: Improving the Accuracy of Protein Side Chain and Backbone Parameters from ff99SB., J Chem Theory Comput. 11 (2015) 3696-3713.
[44] P. Zhou, F. Tian, F. Lv, Z. Shang, Geometric characteristics of hydrogen bonds involving sulfur atoms in proteins., Proteins Struct Funct Bioinf. 76 (2009) 151–163.
[45] U.A. Zitare, J. Szuster, M.C. Santalla, M.E. Llases, M.N. Morgada, A.J. Vila, D.H. Murgida, Fine Tuning of Functional Features of the CuA Site by Loop-Directed Mutagenesis, Inorg. Chem. 58 (2019) 2149–2157. https://doi.org/10.1021/acs.inorgchem.8b03244.
[46] S. Döpner, P. Hildebrandt, F.I. Rosell, A.G. Mauk, Alkaline Conformational Transitions of Ferricytochrome c Studied by Resonance Raman Spectroscopy, J. Am. Chem. Soc. 120 (1998) 11246–11255. https://doi.org/10.1021/ja9717572.
[47] H.K. Ly, M.A. Martí, D.F. Martin, D. Alvarez-Paggi, W. Meister, I.M. Weidinger, P. Hildebrandt, D.H. Murgida, Thermal Fluctuations Determine the Electron-Transfer Rates of Cytochrome c in Electrostatic and Covalent Complexes, ChemPhysChem. 11 (2010) 1225–1235.
[48] L. Tognaccini, C. Ciaccio, V. D'Oria, M. Cervelli, B.D. Howes, M. Coletta, P. Mariottini, G. Smulevich, L. Fiorucci, Structure–function relationships in human cytochrome c: The role of tyrosine 67, J. Inorg. Biochem. 155 (2016) 56–66. https://doi.org/10.1016/j.jinorgbio.2015.11.011.
[49] G. Battistuzzi, C.A. Bortolotti, M. Bellei, G. Di Rocco, J. Salewski, P. Hildebrandt, M. Sola, Role of Met80 and Tyr67 in the Low-pH Conformational Equilibria of Cytochrome c, Biochemistry. 51 (2012) 5967–5978. https://doi.org/10.1021/bi3007302.

[50] T. Ying, Z.-H. Wang, Y.-W. Lin, J. Xie, X. Tan, Z.-X. Huang, Tyrosine-67 in cytochrome c is a possible apoptotic trigger controlled by hydrogen bonds via a conformational transition, Chem. Commun. (2009) 4512–4514. https://doi.org/10.1039/B904347K.
[51] T.L. Luntz, A. Schejter, E.A. Garber, E. Margoliash, Structural significance of an internal water molecule studied by site-directed mutagenesis of tyrosine-67 in rat cytochrome c, Proc. Natl. Acad. Sci. 86 (1989) 3524. https://doi.org/10.1073/pnas.86.10.3524.
[52] H. Maity, J.N. Rumbley, S.W. Englander, Functional role of a protein foldon—An Ω-loop foldon controls the alkaline transition in ferricytochrome c, Proteins Struct. Funct. Bioinforma. 63 (2006) 349–355. https://doi.org/10.1002/prot.20757.
[53] D. Alvarez-Paggi, D.F. Martín, P.M. Debiase, P. Hildebrandt, M.A. Martí, D.H. Murgida, Molecular basis of coupled protein and electron transfer dynamics of cytochrome c in biomimetic complexes, J. Am. Chem. Soc. 132 (2010) 5769–5778. https://doi.org/10.1021/ja910707r.
[54] J. Montero, M. Mari, A. Colell, A. Morales, G. Basañez, C. Garcia-Ruiz, J.C. Fernández-Checa, Cholesterol and peroxidized cardiolipin in mitochondrial membrane properties, permeabilization and cell death, Biochim. Biophys. Acta BBA - Bioenerg. 1797 (2010) 1217–1224. https://doi.org/10.1016/j.bbabio.2010.02.010.
[55] D.H. Murgida, P. Hildebrandt, Electron-transfer processes of cytochrome c at interfaces. New insights by surface-enhanced resonance Raman spectroscopy, Acc. Chem. Res. 37 (2004) 854–861. https://doi.org/10.1021/ar0400443.
[56] E. Laviron, General expression of the linear potential sweep voltammogram in the case of diffusionless electrochemical systems, J. Electroanal. Chem. Interfacial Electrochem. 101 (1979) 19–28. https://doi.org/10.1016/S0022-0728(79)80075-3.
[57] A. Kranich, H.K. Ly, P. Hildebrandt, D.H. Murgida, Direct observation of the gating step in protein electron transfer: Electric-field-controlled protein dynamics, J. Am. Chem. Soc. 130 (2008) 9844–9848. https://doi.org/10.1021/ja8016895.
[58] S. Gosavi, R.A. Marcus, Nonadiabatic Electron Transfer at Metal Surfaces, J. Phys. Chem. B. 104 (2000) 2067–2072.
[59] R.A. Marcus, N. Sutin, Electron transfers in chemistry and biology, BBA Rev. Bioenerg. 811 (1985) 265–322. https://doi.org/10.1016/0304-4173(85)90014-X.
[60] H. Yue, D. Khoshtariya, D.H. Waldeck, J. Grochol, P. Hildebrandt, D.H. Murgida, On the Electron Transfer Mechanism Between Cytochrome c and Metal Electrodes. Evidence for Dynamic Control at Short Distances, J. Phys. Chem. B. 110 (2006) 19906–19913. https://doi.org/10.1021/jp0620670.
[61] U.A. Zitare, J. Szuster, M.F. Scocozza, A. Espinoza-Cara, A.J. Leguto, M.N. Morgada, A.J. Vila, D.H. Murgida, The role of molecular crowding in long-range metalloprotein electron transfer: Dissection into site- and scaffold-specific contributions, Electrochimica Acta. 294 (2019) 117–125. https://doi.org/10.1016/j.electacta.2018.10.069.
[62] D.E. Khoshtariya, T.D. Dolidze, L.D. Zusman, D.H. Waldeck, Observation of the Turnover between the Solvent Friction (Overdamped) and Tunneling (Nonadiabatic) Charge-Transfer Mechanisms for a Au/Fe(CN)63-/4- Electrode Process and Evidence for a Freezing Out of the Marcus Barrier, J. Phys. Chem. A. 105 (2001) 1818–1829. https://doi.org/10.1021/jp0041095.
[63] D.V. Matyushov, Dynamical Effects in Protein Electrochemistry, J. Phys. Chem. B. 123 (2019) 7290–7301. https://doi.org/10.1021/acs.jpcb.9b04516.

[64] M.M.G. Krishna, Y. Lin, J.N. Rumbley, S. Walter Englander, Cooperative Omega Loops in Cytochrome c: Role in Folding and Function, J. Mol. Biol. 331 (2003) 29–36. https://doi.org/10.1016/S0022-2836(03)00697-1.

Graphical Table of Contents Entry